Electronic Supplementary Information (ESI)

Anchor and Space-Confinement Effects to Form Ultrafine Ru Nanoclusters for Efficient Hydrogen Generation

Jian Yang[a], Heng Guo[a], Shulin Chen[c], Yulan Li[a], Chao Cai[b], Peng Gao[c], Liping Wang[a], Yanning Zhang[b], Rujie Sun[d], Xiaobin Niu*[, a], Zhiming Wang[b]

[a]School of Materials and Energy, State Key Laboratory of Electronic Thin Film and Integrated Devices, University of Electronic Science and Technology of China, Chengdu 610054, China

[b]Institute of Fundamental and Frontier Sciences, University of Electronic Science and Technology of China, Chengdu 610054, P. R. China

[c]Collaborative Innovation Center of Quantum Matter, Beijing 100871, China

[d]Wavetronix LLC, Provo, UT 84606, USA

[*] Corresponding author: xbniu@uestc.edu.cn

1. Experimental Section

1.1. Chemicals.

$RuCl_3$, 4-nitrophthalonitrile, melamine, sodium sulfide, K_2HPO_4, KH_2PO_4, KOH and KCl were purchased from Adamas-beta®. 1-Methyl-2-pyrrolidinone (NMP), N, N-Dimethylformamide (DMF), H_2SO_4, HCl, alcohol, and acetone were supplied by Chengdu Kelong Chemicals Co., Ltd. 5% of Nafion and Pt/C (20wt%) were from Sigma-Aldrich and Johnson Matthey company, respectively. All the reagents were analytical grade and used as received. Ultrapure water is supplied by a Millipore system. Graphene oxide (GO, purity>99 wt%, layers: <3, thickness: 0.5-1.2 nm, diameter: 0.5-3.0 mm) was offered from Chengdu Organic Chemicals Co. Ltd., Chinese Academy of Sciences.

1.2. Material synthesis.

Ruthenium tetranitrophthalocyanine (RuPc-NO_2) synthesis. RuPc-NO_2 was synthesized using a previously developed method.[1] Typically, 7.54 g 4-nitrophthalonitrile (43 mmol) and 2.25g $RuCl_3$ (approximate 11mmol) were mixed in a 100 mL four-necked round-bottom flask equipped with condensator and mechanical stirrer. The mixture was heated to 140 ^oC with stirring to form a slurry, then maintained at 160 ^oC for 4h under argon atmosphere with constant stirring. After cooling to room temperature, the solid crude production was ground into fine powders in agate mortar. Then, the product was immersed in 1M HCl and 1M NaOH for 8h, successively, and filtered by water and methanol. For further refining purer product, the RuPc-NO_2 was treated by Soxhlet extractor with methanol and acetone for 2 days respectively and dried at 60 ^oC in a vacuum oven for 24h to obtain 6.08 g of a bluish green solid. Analysis for $C_{32}H_{12}N_{12}O_8Ru$ (793g mol^{-1}): Calc. (%) C, 48.4; H, 1.5; N, 21.2; O, 16.1; Ru, 12.8. Found: C, 45.1; H, 4.2; N, 14.1; O, 23.8; Ru, 12.8. IR absorption peaks (cm^{-1}): 733, 811, 850, 909, 1090, 1109, 1144, 1257, 1338, 1405, 1490, 1526, 1610, 1647, 1734, 1898, and 3089. Electronic absorption, λmax (nm): 355, 600, 665.

Ruthenium tetraaminephthalocyanine (RuPc-NH_2) synthesis. The synthesis of RuPc-NH_2

was carried out via reducing nitro of RuPc-NO_2 using sodium sulphide ($Na_2S•9H_2O$). A total of 4.0 g RuPc-NO_2 was dissolved in 150 mL of DMF solvent and subsequent 18 g of $Na_2S•9H_2O$ was added and stirred at 60^oC for 8h. The product was poured into water and collected by filtration and washed with water for several times until the filtrate is neutral on litmus paper. The product was dried in the oven at 60^oC for overnight to obtain about 3.21g of a dark bluish powder. Analysis for $C_{32}H_{20}N_{12}Ru$ (673 g mol^{-1}): Calc. (%) C, 57.1; H, 3.0; N, 25.0; Ru, 15.0. Found; C, 55.2; H, 4.1; N, 24.2; Ru, 16.5. IR absorption peaks (cm^{-1}): 743, 830, 1046, 1112, 1258, 1331, 1398, 1489, 1603, 1717, 1770, 3216, and 3424. Electronic absorption, λmax (nm): 317, 634~682nm.

Graphitic carbon nitride (g-CN) synthesis. 10.0 g melamine was placed into a ceramic crucible with a cover and heated to 550 ^oC at a heating rate of 2.3^oC min^{-1} and then maintained at 550^oC for 4 hours before being cooled down to room temperature. The yellow bulk g-CN product was ground to fine powder in mortar. For preparing thin layers of g-CN, 2.0 g of bulk g-CN synthesized was dispersed into 100 mL of methanol under sonication for one week in an intermittent process. The upper layer suspension was transferred to beaker and then g-CN nanosheet was obtained by evaporate solvent at 60^oC.

Preparation of Ru@NG. 0.1 g RuPc-NH_2 was added into 10 mL of deionized water, and then 2.5 mL of GO solution (2.0 mg/mL) was dropwise added into the above-mentioned solution. The mixture was placed into a sonic bath for two hours to obtain a homogeneous suspension and evaporated at 80 ^oC overnight to form homogeneous powders. The solid mixture was then annealed at 800 ^oC for 2h under argon atmosphere (99.999%) in the quartz tube at a heating rate of 5 ^oC min^{-1}. After that, the black powder was collected, washed with ethanol and water several times to remove the residue of reactants, and finally dried in a vacuum at 60 ^oC overnight. At last, the obtained catalyst is Ru@NG with 5.0 wt% content of GO.

Preparation of Ru@NC. Ru@NC was also prepared via the same process as Ru@NG

without adding any GO solution, only a single precursor RuPc-NH_2.

Preparation of Ru@N-g-CN. Ru@N-g-CN was also obtained via the same process as Ru@NG, only replaced the GO by g-CN nanosheets. The amount of g-CN is also 5.0 wt%.

Preparation of Ru/NC. Ru/NC was prepared by direct carbonization of $RuCl_3$ (0.3g, 1.5mmol) and 4-nitrophthalonitrile (1.04 g, 6.0mmol) mixture under the same process.

Ru nanoparticles (Ru-np) synthesis. 100 mg $NaBH_4$ was dissolved in 20 ml deionized water under an intense stirring**,** then 20 ml $RuCl_3$ solution (5mg ml^{-1}) was added to the above $NaBH_4$ solution dropwise by an injector. After stirring for 20h, the precipitated black Ru nanoparticles were collected by evaporating the water and rinsed several times by distilled water and ethanol, and finally dried in an oven at 60 ^oC.

1.3. Preparation of the working electrode

4.0 mg of the catalyst powder was dispersed into 980 uL of water/ethanol mixed solvents (volume ratio is 4:1) and 20 uL of 5wt% Nafion solution under sonication. Thereafter, 15 uL of the obtained homogeneous catalyst ink was dropped onto a mirror polished glassy carbon electrode (3mm in diameter). In order to avoid catalysts' detachment during electrochemical measurement, 1.0 uL 0.5% Nafion was dropped onto the dried catalyst coating. The other control samples were prepared by the same procedure. The loading amount of catalyst is about 850 ug cm^{-2} for all the working electrodes.

1.4. Materials characterization

Fourier transformed infrared (FTIR) spectra were recorded by Bluke VERTEX 80. The measured wafer was prepared as KBr pellet with the weight ratio of sample to KBr, 1/100. Powder X-ray diffraction (XRD) measurements were performed on Bruker D8 Advance diffractometer with CuKa1 radiation (λ=0.15406 nm). The absorption spectra were recorded on an ultraviolet-visible (UV-Vis) photospectrometer (TU-1810, Persee). Thermogravimetric analysis (TGA) was carried out using TA Q50 system under air atmosphere at a heating rate of 20 ^oC/min from room temperature to 800 ^oC and held at 800 ^oC for 20min. The

morphologies and structures of samples were characterized using field-emission scanning electron microscopy (FESEM; Hitachi SU-8010). Transmission electron microscopy (TEM), high-angle annular dark-field (HADDF) scanning transmission electron microscopy (STEM) and bright field (BF) images were acquired using an aberration-corrected FEI Titan Themis G2 microscope operated at an accelerating voltage of 80 kV to minimize the electron beam induced damage. STEM images were acquired with a beam current of 100pA, a convergence semi-angel of 25 m-rad, and a collection semi-angle snap in the range of 53-260 m-rad.Raman scattering measurements were performed using a multichannel modular triple Raman system, with confocal microscopy at room temperature and an excitation wavelength of 532 nm. The Brunauer-Emmett-Teller (BET) specific surface area was determined by nitrogen adsorption-desorption isotherm measurements at 77 K (NOVA 2200e). XPS measurements were performed on an X-ray photoelectron spectrometer (Thermo ESCALAB 250).

1.5. Electrochemical measurements

All electrochemical measurements were performed on the CHI760E (CH Instruments, Inc., Shanghai) electrochemical workstation in a three-electrode system. In order to avoid the effect of Pt deposition on HER, a graphite rod was used as the counter electrode in all electrochemical measurements. An Ag/AgCl (saturated KCl solution) was used as the reference electrode in all measurements. The reference electrode was also calibrated, and all potentials were referenced to a reversible hydrogen electrode (RHE). All the polarization curves were obtained at a scan rate of 2mV s^{-1} after 100 cycles of Cyclic Voltammetry (CV) in Ar saturated electrolyte.

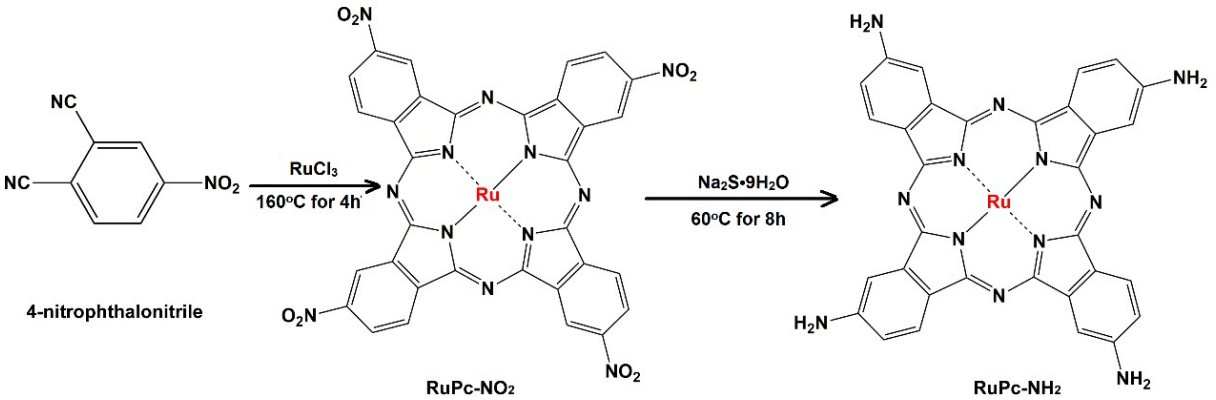

Figure. S1. Synthetic route and structure of RuPc-NH_2 used in this study. 4-Nitrophthalonitrile and $RuCl_3$ reacted in melting state to form RuPc-NO_2, while the $Na_2S{\cdot}9H_2O$ serve as reducing agent to obtain RuPc-NH_2. The Ru atoms are anchored in the center of N_4-macrocycle by chemical bond.

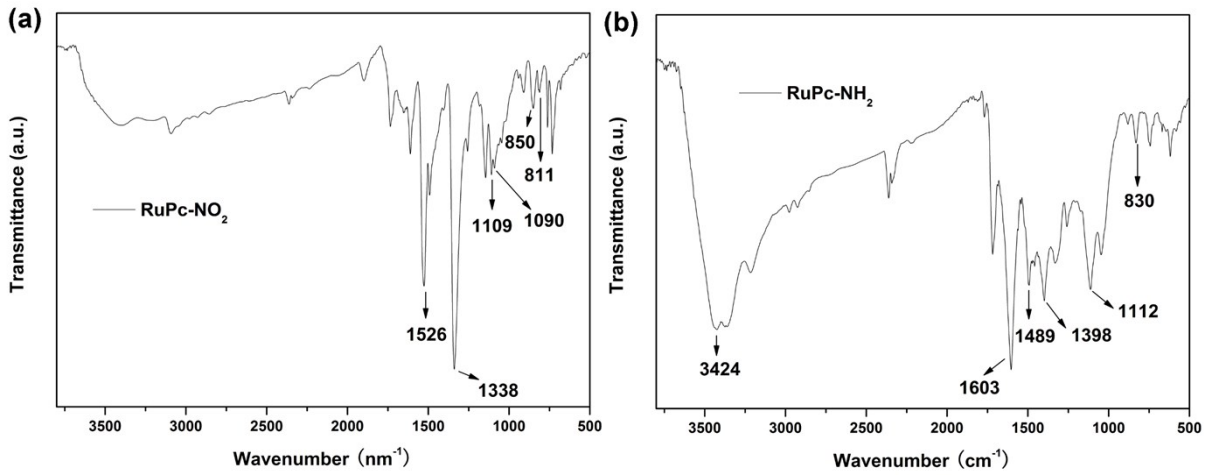

Figure. S2. The FTIR spectra of RuPc-NO_2 and RuPc-NH_2, respectively. (**a**) The peaks at 1109, 1090, 850 and 811cm^{-1} belong to the skeleton vibration of phthalocyanine ring, the peaks 1526 and 1338cm^{-1} are the symmetrical and anti-symmetric stretching vibration absorption peaks of $–NO_2$ group. (**b**) The absorption peak of nitro is almost disappeared, the peak at 3424 cm^{-1} is attributed to amino group.

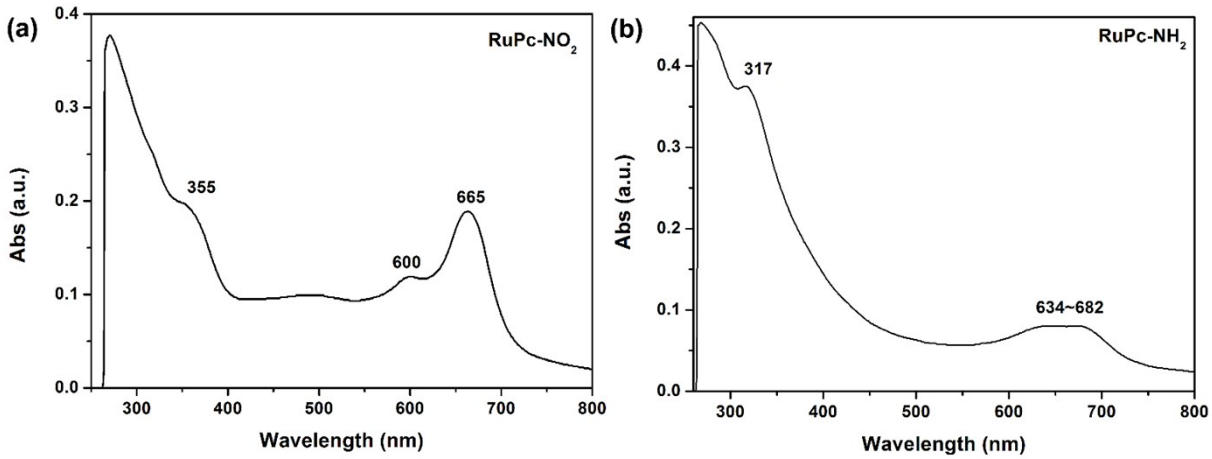

Figure. S3. (**a** and **b**) The UV-vis absorption characteristics of RuPc-NO_2 and RuPc-NH_2 were confirmed by UV-vis spectrophotometer.

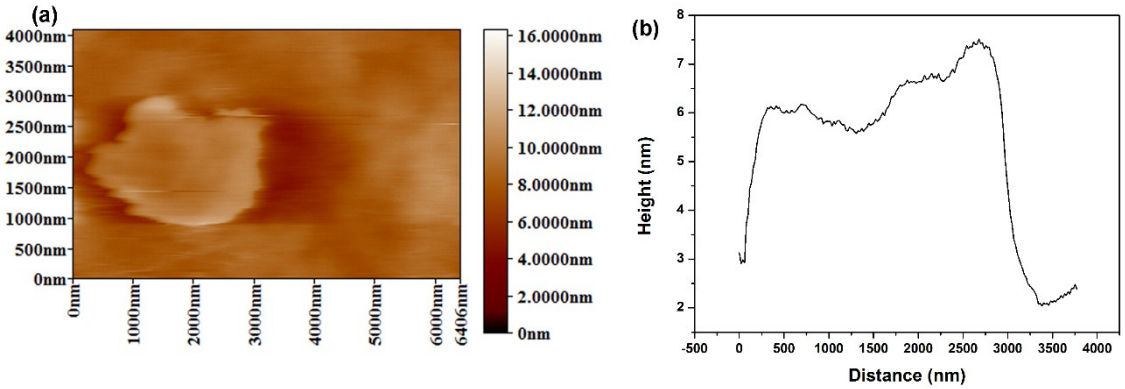

Figure. S4. (**a**) AFM image of g-CN nanosheets and (**b**) corresponding height profiles. The size of g-CN nanosheet is about 2760 nm, and the height is about 6 nm, indicating the successfully exfoliating g-CN nanosheet.

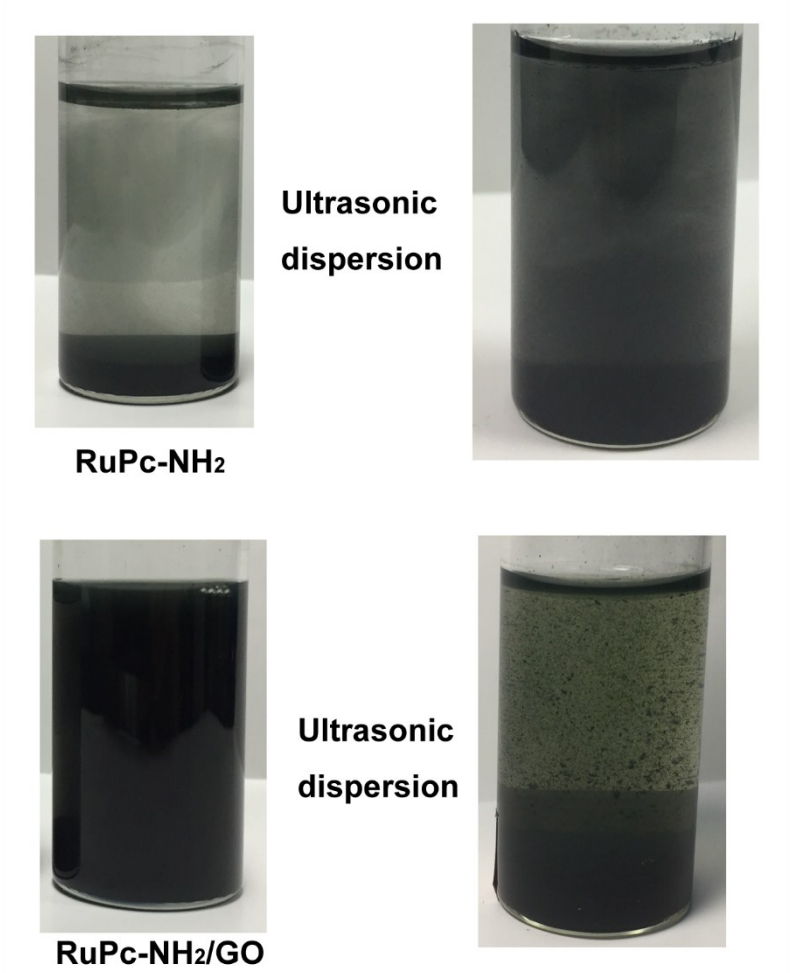

Figure. S5. Photograph of RuPc-NH_2, RuPc-NH_2/GO aqueous suspension before and after ultrasonic dispersion. Before ultrasonic treatment, the RuPc-NH_2 are precipitated to the bottom, while the RuPc-NH_2/GO are dispersed in aqueous solution uniformly. This is probable due to the interaction between the amino and carbonyl groups. After ultrasonic treatment and half an hour standing, both the RuPc-NH_2 and RuPc-NH_2/GO are precipitated to the bottom. Interestingly, the volume of RuPc-NH_2/GO is obviously higher than RuPc-NH_2, which is ascribed to high surface area of GO.

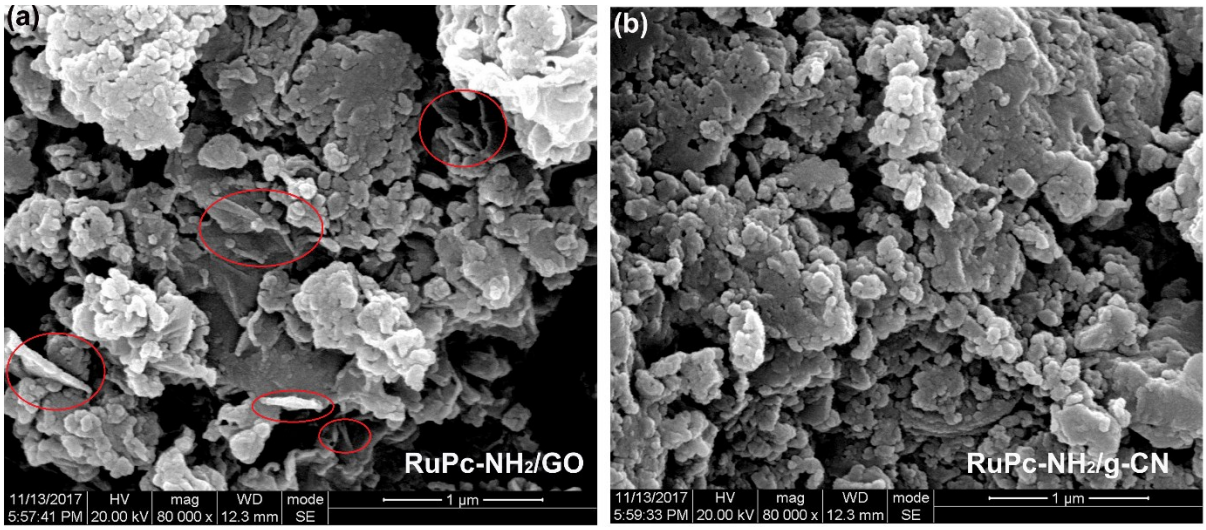

Figure. S6. SEM images of RuPc-NH_2/GO (**a**) and RuPc-NH_2/g-CN (**b)** mixtures. In the Figure. S6**a**, the layer structures can be observed in the red areas.

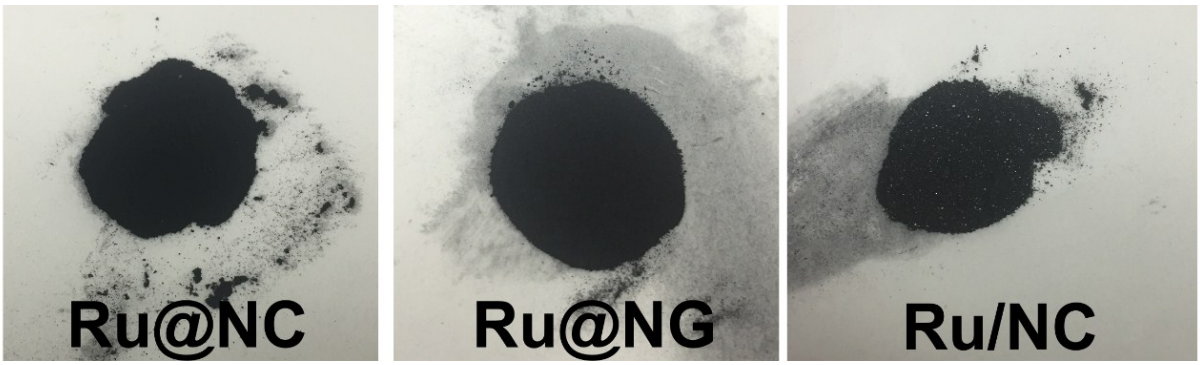

Figure. S7. The photograph of as-prepared catalysts for Ru@NC, Ru@NG, and the control sample Ru/NC.

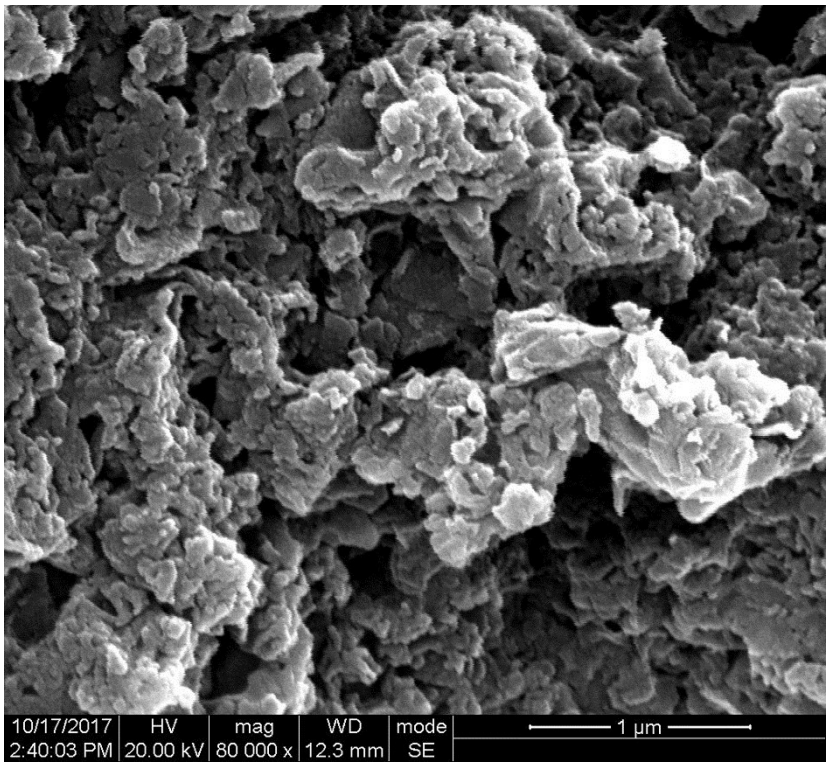

Figure. S8. SEM image of Ru@NG catalyst

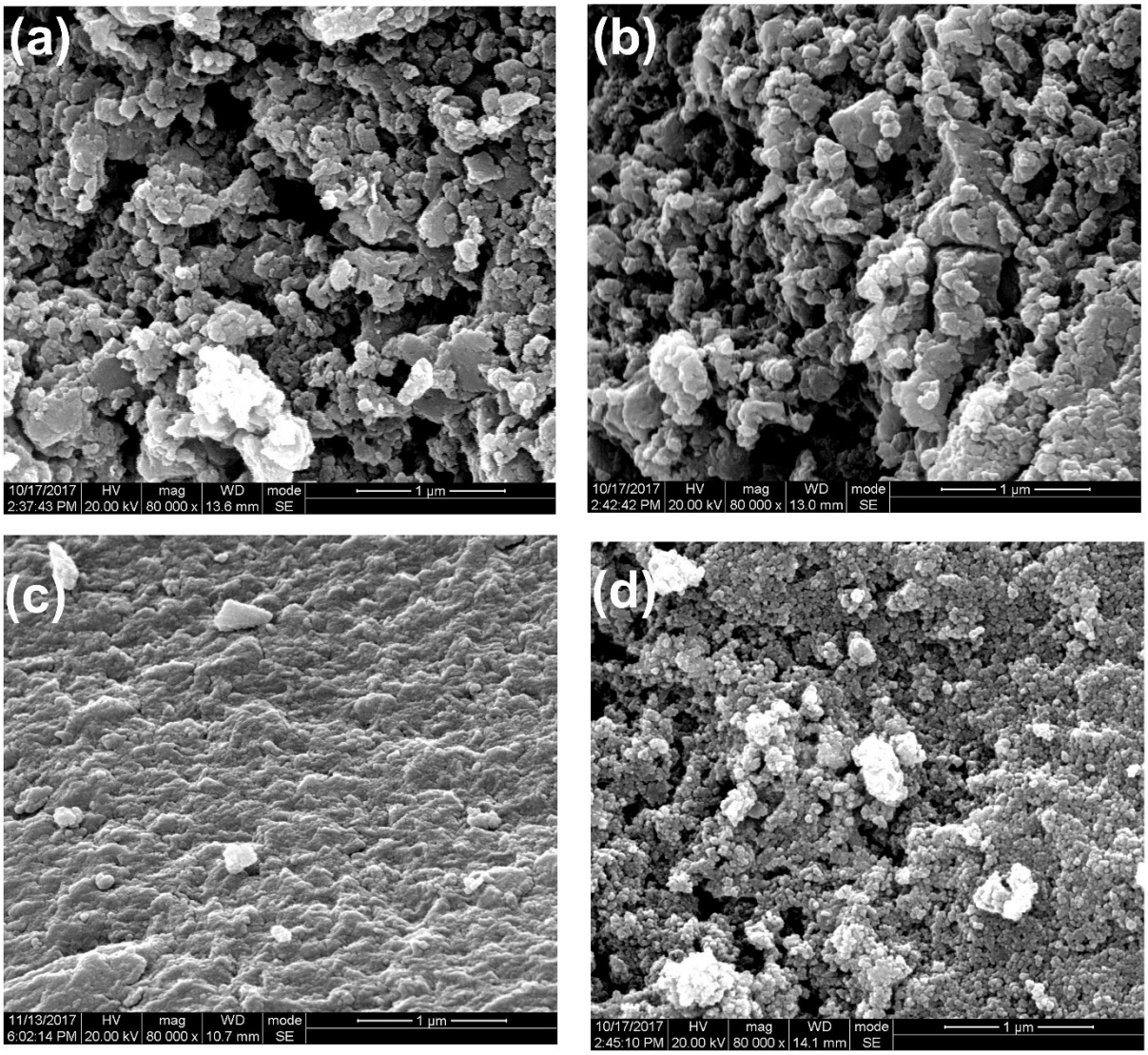

Figure. S9. SEM images of catalysts, corresponding to Ru@NC (**a**), Ru@N-g-CN (**b**), Ru/NC (**c**) and Ru-np (**d**) respectively.

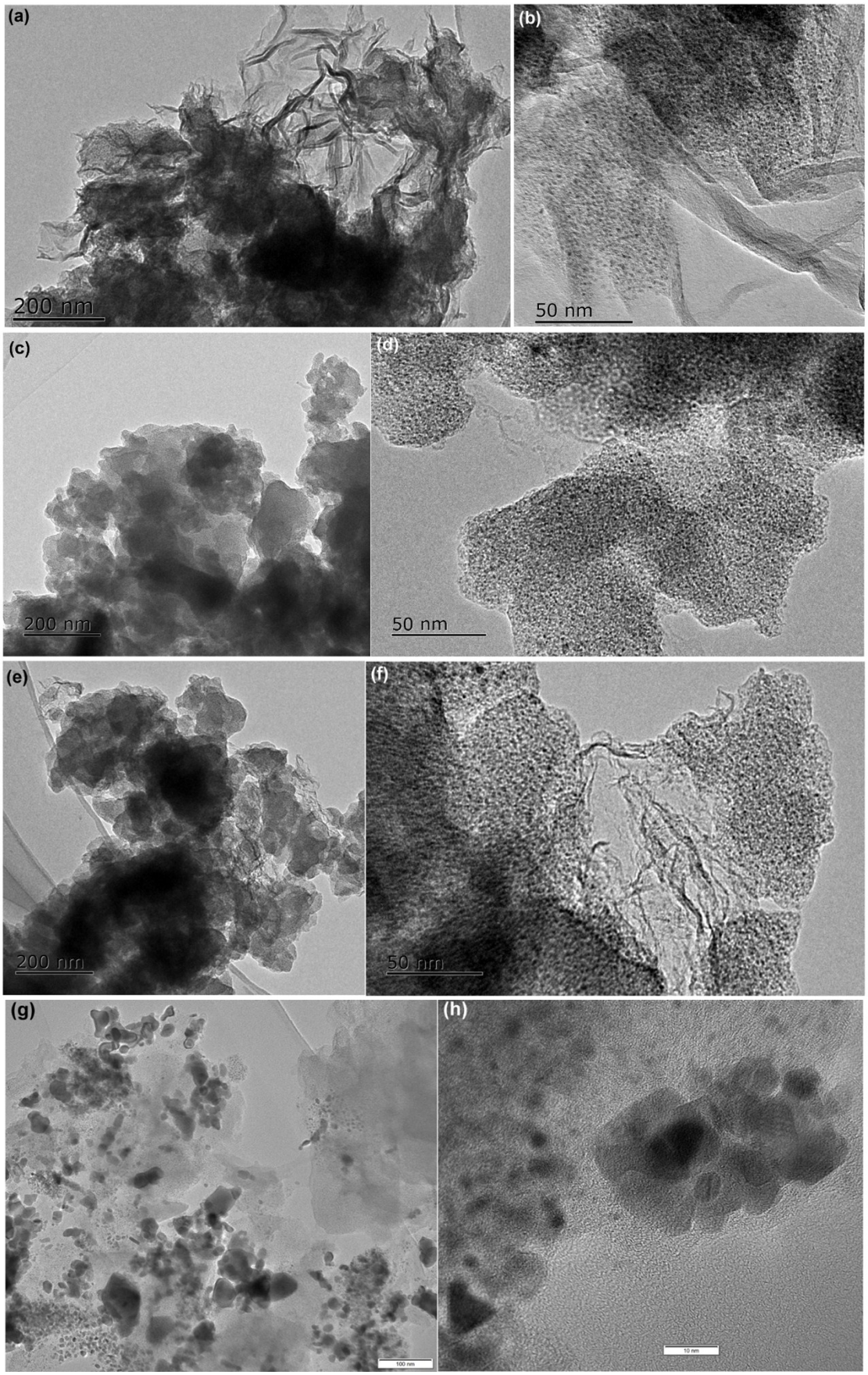

Figure. S10. TEM images of Ru@NG (**a, b**), Ru@NC (**c, d**), Ru@N-g-CN (**e, f**) at 200 nm and 50nm scale bar, and Ru/CN (**g, h**) at 200 nm and 10nm scale bar respectively.

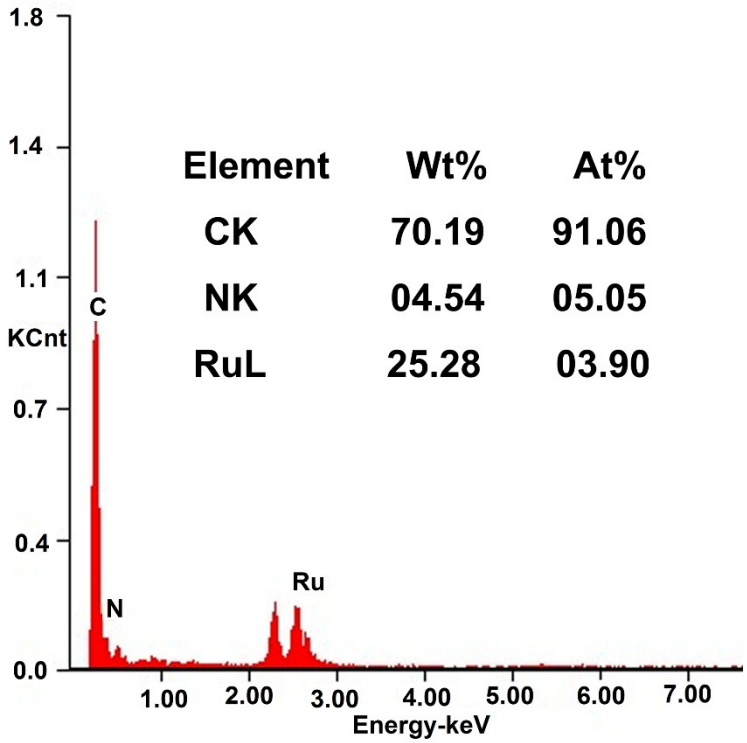

Figure. S11. EDX spectra of Ru@NG.

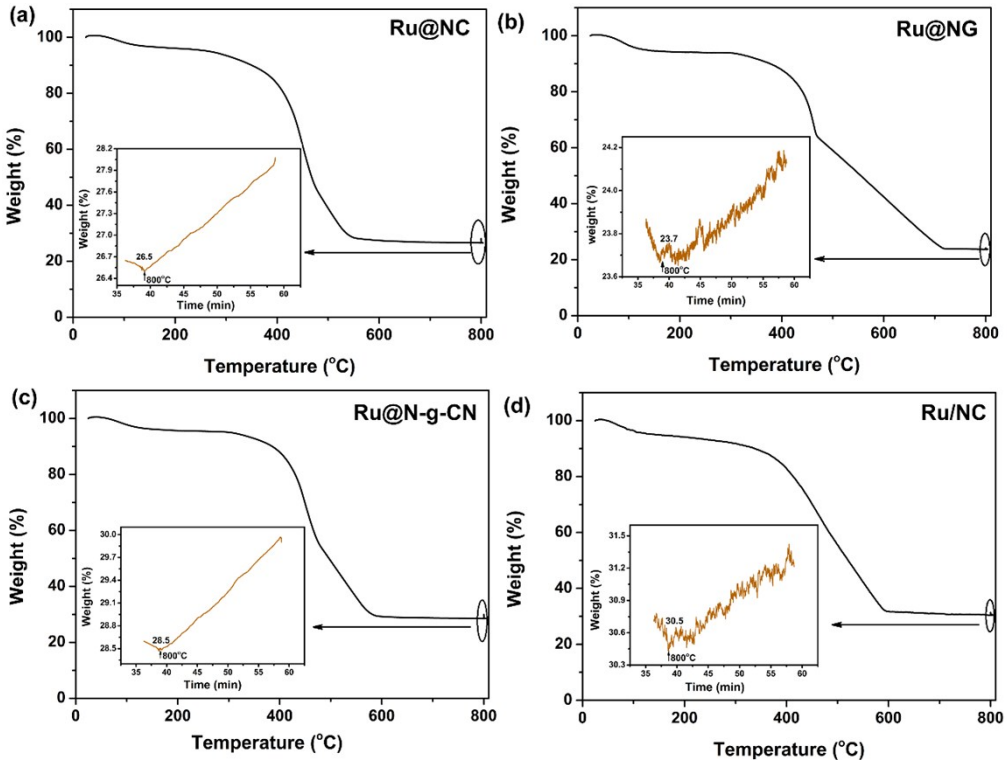

Figure. S12. (**a-d**) TGA curves of as-prepared Ru-based catalysts under air atmosphere with a ramping rate of 20 ^{o}C min^{-1} from room temperature to 800 ^{o}C, then maintains at 800 ^{o}C for 20 min. The insets are the weight-time curves during 800 ^{o}C. We presume the weight nadir is the content of Ru metal in carbonaceous catalysts. The increase of weight is ascribed the oxidation of Ru.

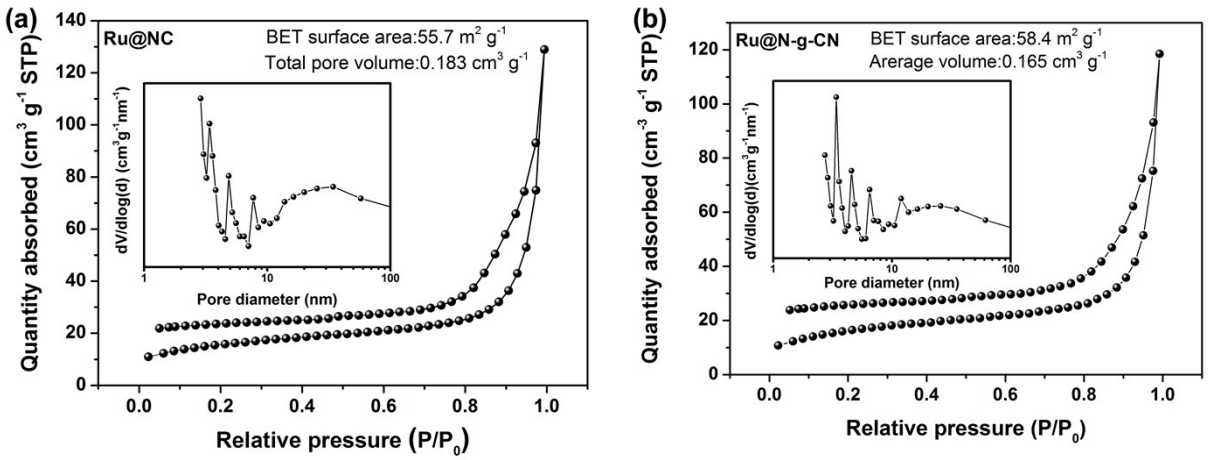

Figure. S13. N_2 adsorption isotherms of Ru@NC (**a**) and Ru@N-g-CN (**b**), respectively. The insets are the corresponding pore size distribution. The pore size distribution based on BJH analysis shows that the pore sizes are mainly distributed in 2~20nm, demonstrating the presence of mesoporous structure, which will facilitate the HER electrocatalysis.

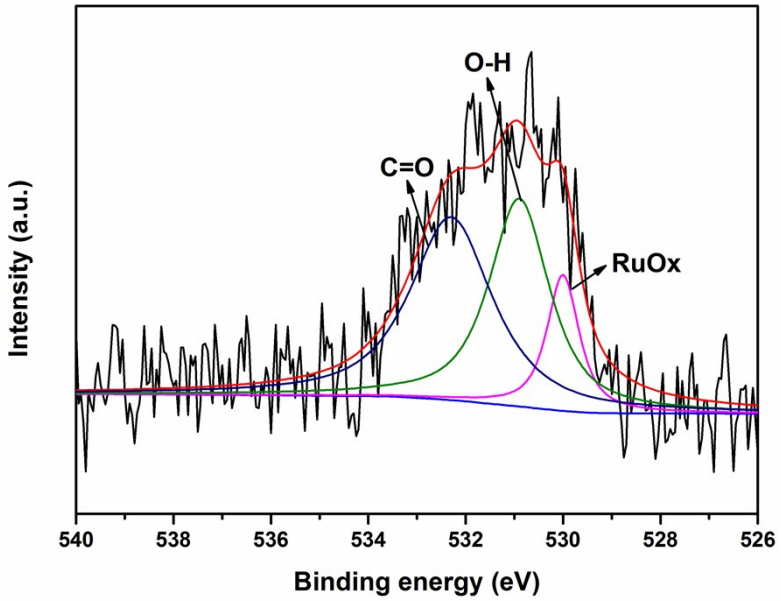

Figure. S14. The High-resolution O 1s spectra of Ru@NG. The peak at 530.0eV belongs to the RuOx on the surface of Ru metal. Meanwhile, the 530.9 and 532.3 eV have been assigned to O-H and C=O respectively.

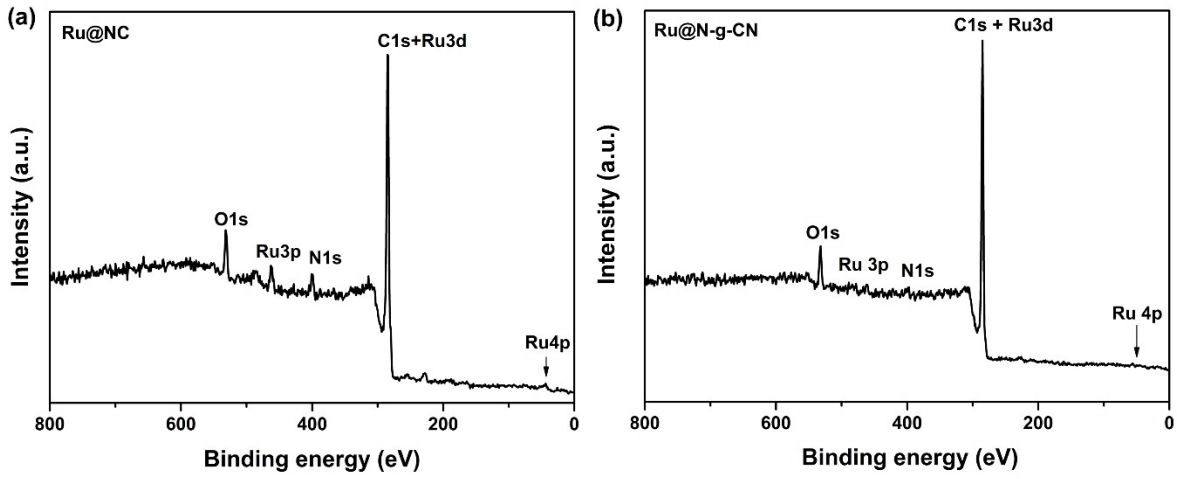

Figure. S15. XPS survey full scan of Ru@NC (**a**) and Ru@N-g-CN (**b**).

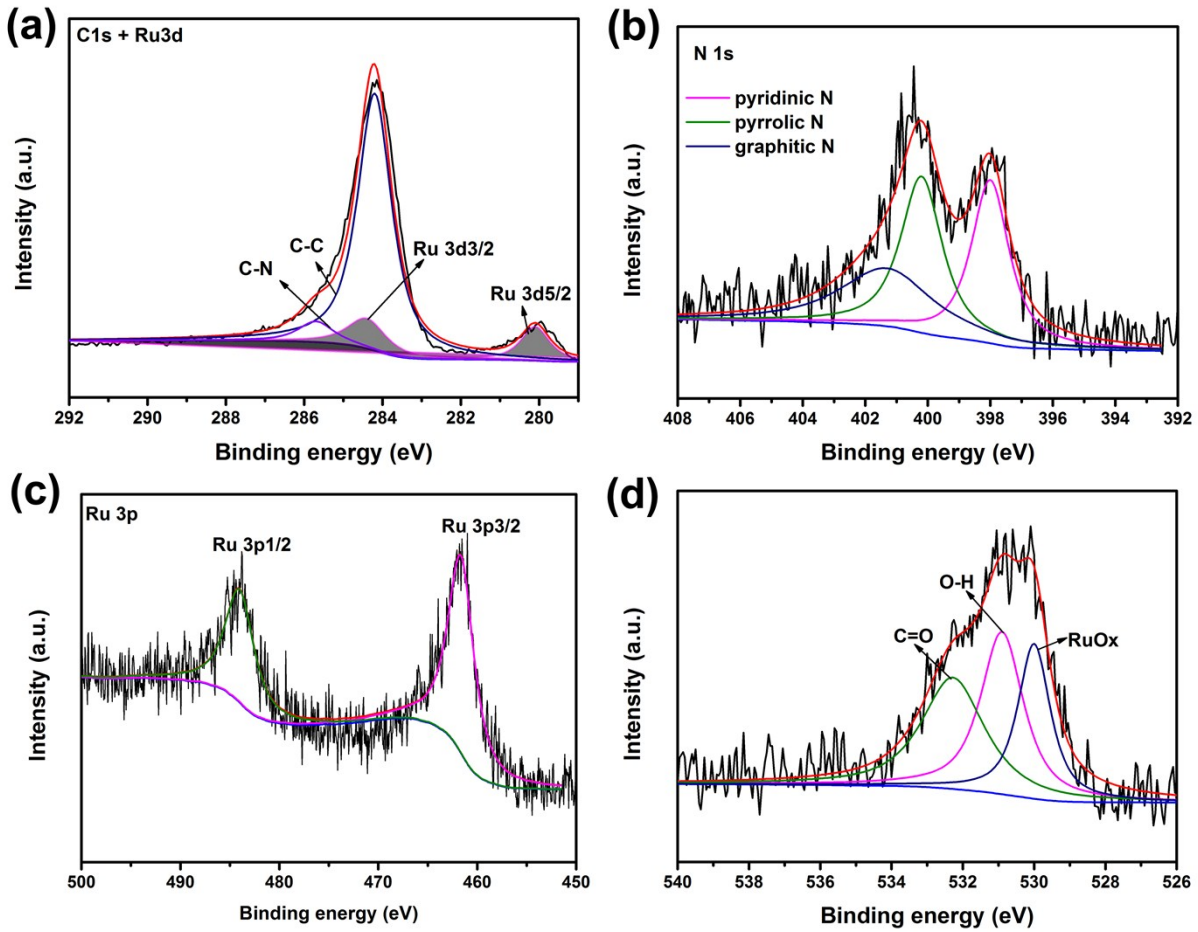

Figure. S16. High-resolution XPS spectra of Ru@NC, corresponding to **(a)** C 1s + Ru 3d, **(b)** N 1s, **(c)** Ru 3p and **(d)** O 1s.

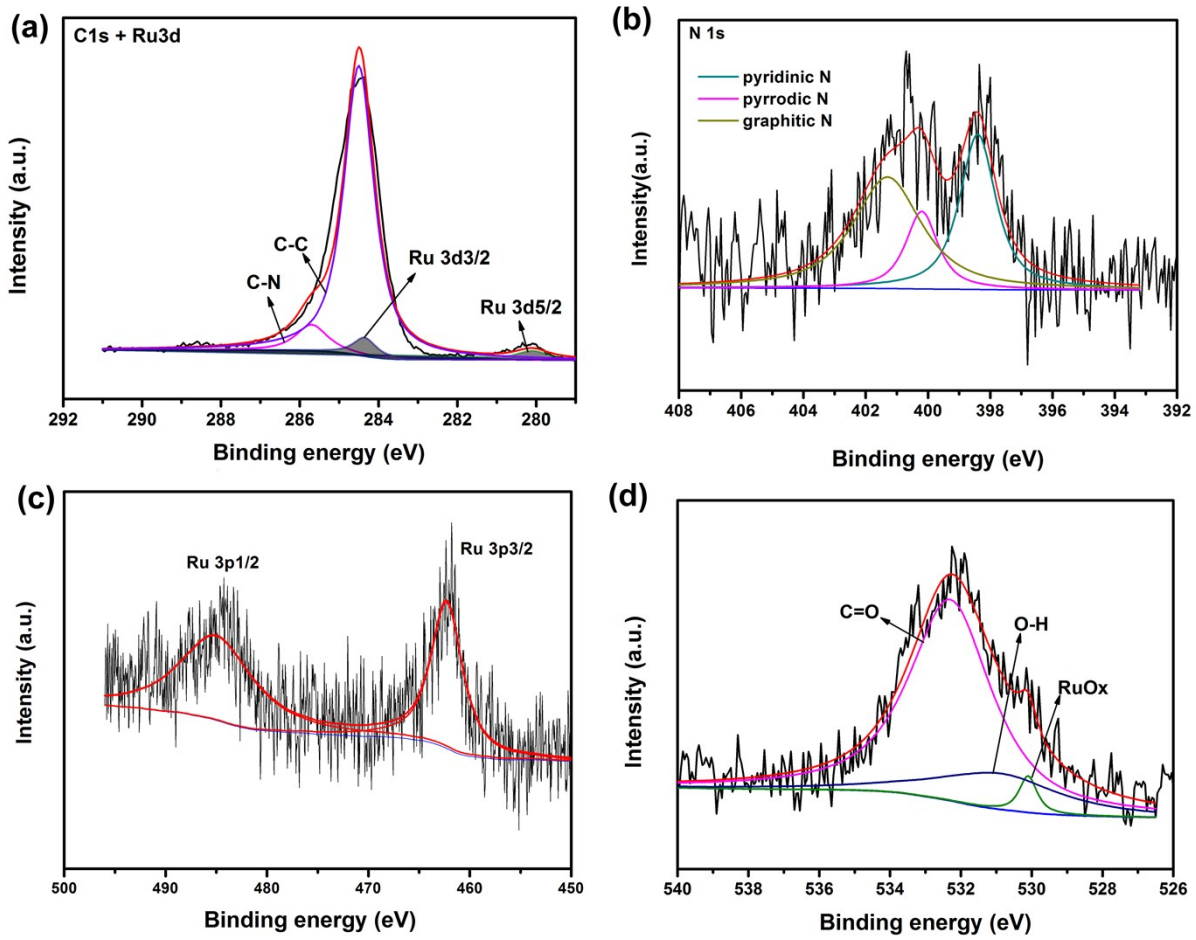

Figure. S17. High-resolution XPS spectra of Ru@N-g-CN, corresponding to **(a)** C 1s + Ru 3d, **(b)** N 1s, **(c)** Ru 3p and **(d)** O 1s. The peaks at 280.1 (Ru3d5/2) and 284.4eV (Ru3d 3/2) are assigned to metal Ru and metal oxide (Ru/RuOx). Meanwhile, the peak at 530.0eV belongs to the RuOx on the surface of Ru metal, the 530.9 and 532.3 eV have been assigned to O-H and C=O respectively.

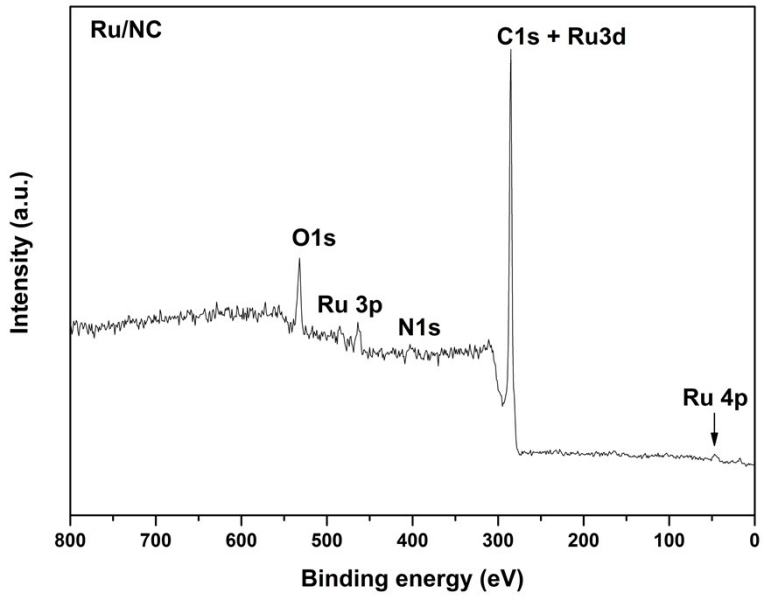

Figure. **S18**. XPS survey full scan of Ru/NC

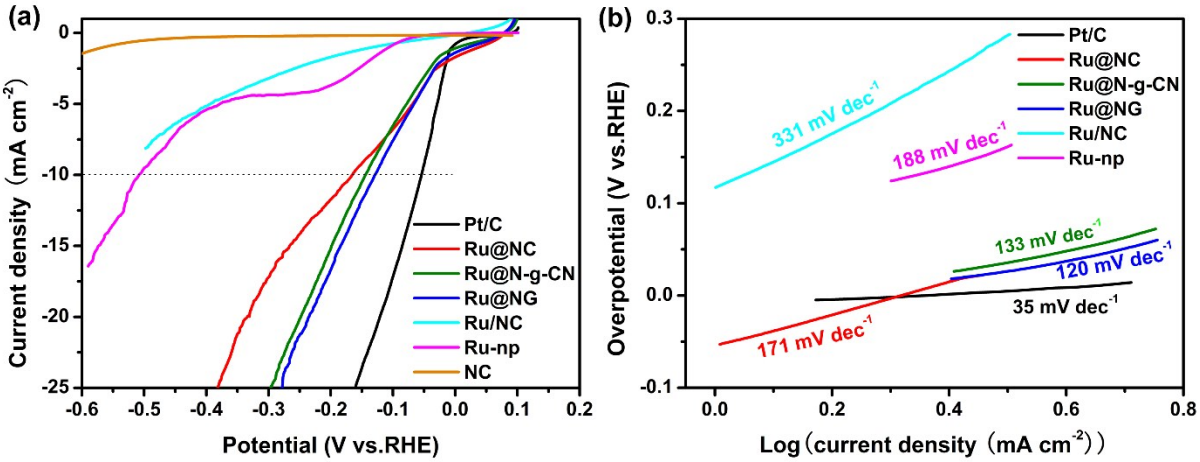

Figure. S19. (**a**) LSV curves of various catalysts in 1.0 M PB solution and (**b**) corresponding Tafel plots.

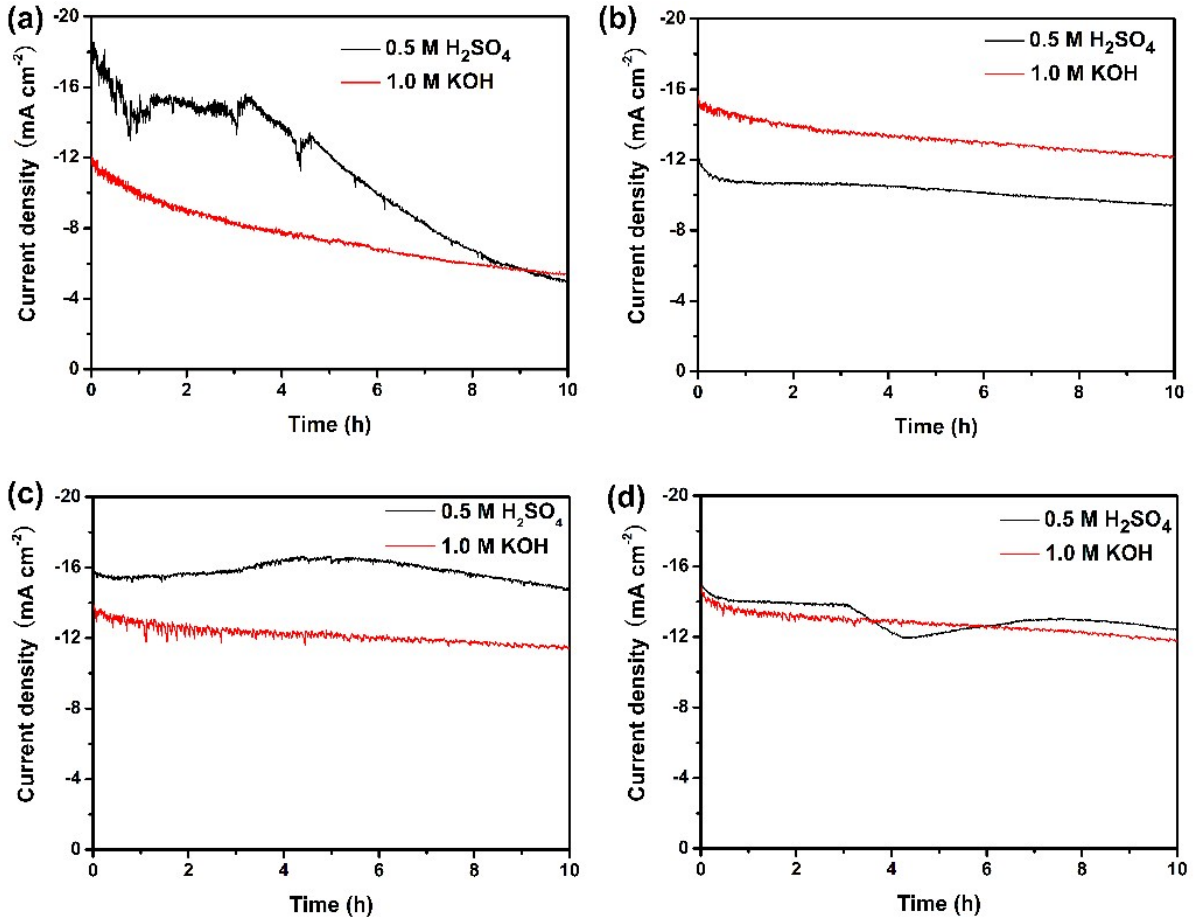

Figure. S20. Time-dependent current density curves of Pt/C (**a**), Ru@NC (**b**), Ru@NG (**c**) and Ru@N-g-CN (**d**) catalysts in acidic and alkaline solution, respectively.

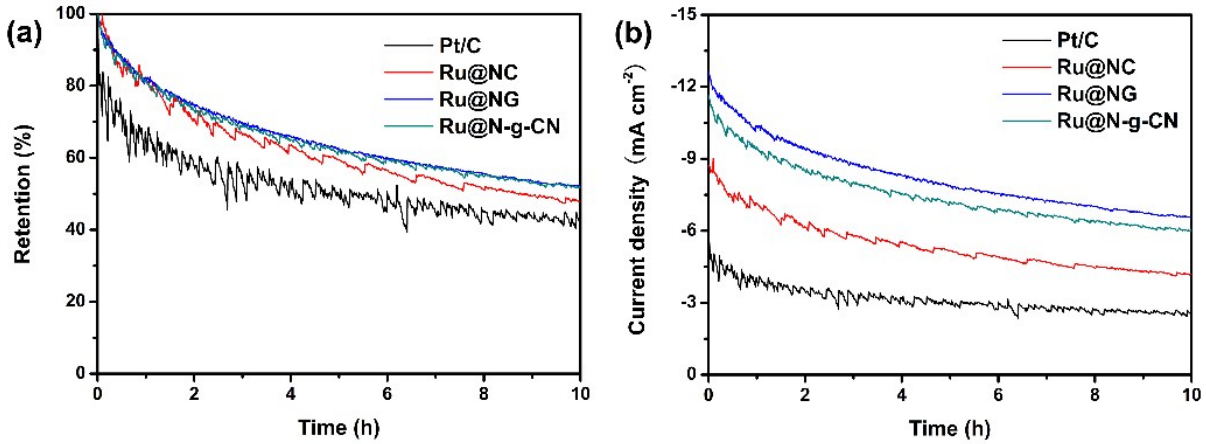

Figure. S21. Time-dependent current density curves of Ru@NC, Ru@NG, Ru@N-g-CN and benchmark Pt/C in 1.0 M PB solution.

Analysis of HER mechanism in alkaline environment

In the HER, there are two kinds of reaction path, either the **Volmer-Heyrovsky** or the **Volmer-Tafel** mechanism. The H* represent one catalytic intermediate, and * denotes a reaction site on the electrode surface.

Volmer step: $H^+ + e^- + * \rightarrow H^*$
Heyrovsky step: $H^* + H^* \rightarrow H_2 + *$
Tafel step: $2H^* \rightarrow H_2 + 2*$
Both in the two reaction routes, the first is Volmer step. If in the acidic condition, the abundant proton source H^+ can quickly adsorb to active sites and generate H* intermediate. Therefore, the catalyst Pt shows the best activity in acidic environment for its more zero closed hydrogen adsorption energy ($\Delta G_H=0$) than other catalysts. However, in basic condition, the proton source is poor, then in order to produce H* in alkaline solution, the H_2O should be adsorbed on the surface of the active sites first and generate M-H_2O (in our catalysis system the active sites are metal Ru nanocluster or metal Pt). Subsequently, the dissociation of the adsorbed H_2O into H atom and adsorbed OH^- should be fast enough to supply protons for the reaction of Volmer step.

Dissociation of H_2O and Volmer step: $M\text{-}H_2O + e^- \rightarrow M\text{-}H^* + OH^-$ (alkaline solution)

In this step, the M-H_2O binding energy should be higher for the attraction between the metal surface and H_2O increasing the proton source supply. This will facilitate the Volmer reaction. The M-H bond needs to be strong enough to expedite M-H* creation. In addition, the M-OH binding energy should be low, making the refresh of the surface much easier and adsorption H_2O again.

The structure and composition of Ru@NG are similar to **Ru@C_2N**, in which ***Baek*** group[8] revealed by DFT that Ru metal and its nanoparticles surfaces have moderate H and H_2O binding energies as well as Pt. However, Ru shows strong attraction to OH compared with Pt. When the Ru nanocluster are embedded into N-doped Carbon in alkaline solution, the bond strengths of H and OH are not significantly different in the presence or absence of N-doped carbon. Importantly, the H_2O binding energy is dramatically increased in Ru@C_2N, enhancing the H_2O capture rate of the Ru nanoparticle. Furthermore, the dissociation of H_2O on the surface of Ru is much easier than that on the surface of Pt, leading to the much faster proton supply for the HER. That's the probable reason why Ru@NG shows superior HER performance than Pt.

The number of exposed active sites (*n*), Electrochemically surface area (ECSA) and Turnover frequency (TOF) measurements:

Underpotential deposition (UPD) of copper has been an effective method for characterizing the active sites of Pt, Ru and Pt-Ru based high-surface area electrocatalysts.[2-3] All the calibration tests were carried out in 0.25 M H_2SO_4 solution containing 10 mM $CuSO_4$, continuously saturated with N_2. Before Cu deposition, the electrode was cycled in pure 0.25 M H_2SO_4 for several scans as the background between 0.05 and 1.05V (vs. RHE) at a scan rate of 10mV s^{-1} with the potential scan ending on the positive-going at 0.05V. The other purpose of the initial treatment was to produce a surface on which virtually all of the Ru was in the reduced state. Then the electrode was polarized at 0.215V (vs. RHE) for 100s to form the UPD layers in 0.25 M H_2SO_4 containing 10 mM $CuSO_4$. Subsequently, the Cu-UPD was stripped from the surface during a positive sweep at 10 mV s^{-1} from 0.215 to 1.05V. The UPD Cu stripping charge (Q_{Cu}) is associated with the anodic peak area subtracting the capacity influence determined in pure 0.25 M H_2SO_4 solution.

In this method, the **n** can be qualified based on the UPD copper stripping charge (*Qcu*, $Cu_{upd} \rightarrow Cu^{2+}+2e^-$) with the following equation: $\mathbf{n}=Q_{Cu}/2F$, F is the Faraday constant (96485C mol^{-1}).

The ECSA is calibrated as following equation:

ECSA(cm^2_{metal} g^{-1}_{metal}) $=Q_{Cu}/(M_{matal} \times 0.42$ mC $cm^{-2})$, where M_{metal} is calculated from the mass loading on a certain geometric area of the working electrode and the Ru content based on TGA data, the value of 0.42mC cm^{-2} is assumed for a saturated Cu-upd monolayer formation on active metal sites, validated for Pt and Ru electrodes surfaces.

The TOF (s^{-1}) is calculated with the following equation:

TOF =I/(2Fn), where I is the current (A) during LSV measurement, F is the Faraday constant (C mol^{-1}), **n** is the number of active sites (mol). The factor $^1/_2$ is based on the consideration that two electrons are required to form one hydrogen molecule.

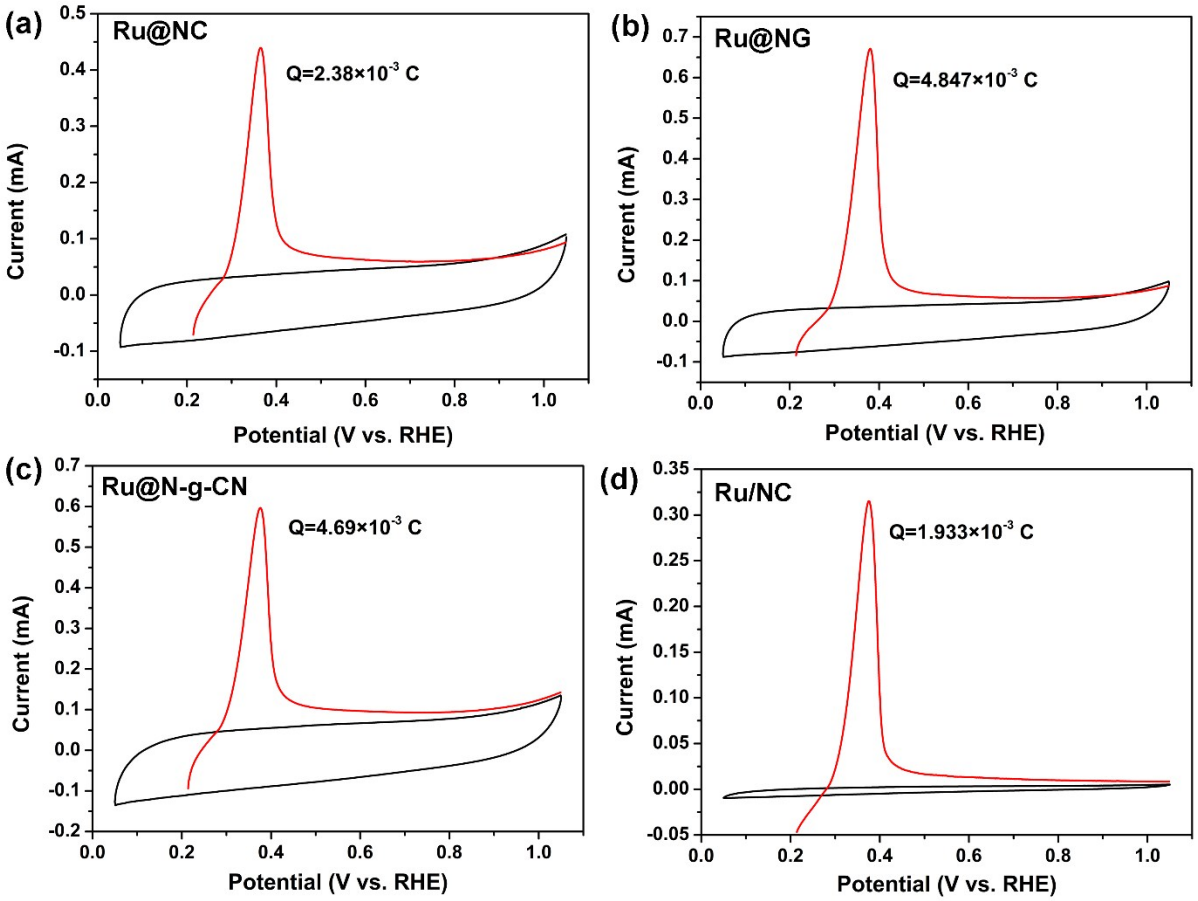

Figure. S22. The Cu-UPD in 0.25 M H_2SO_4 solution containing 10 mM $CuSO_4$ (marked by red lines), the back lines as background are measured in the absence of 10 mM $CuSO_4$. The stripping charge Q_{Cu} are calculated by the following equation: $Q_{Cu}=S/\upsilon$, where S is the area of stripping peak subtracting background (A×V), υ is the scan rate (V/s).

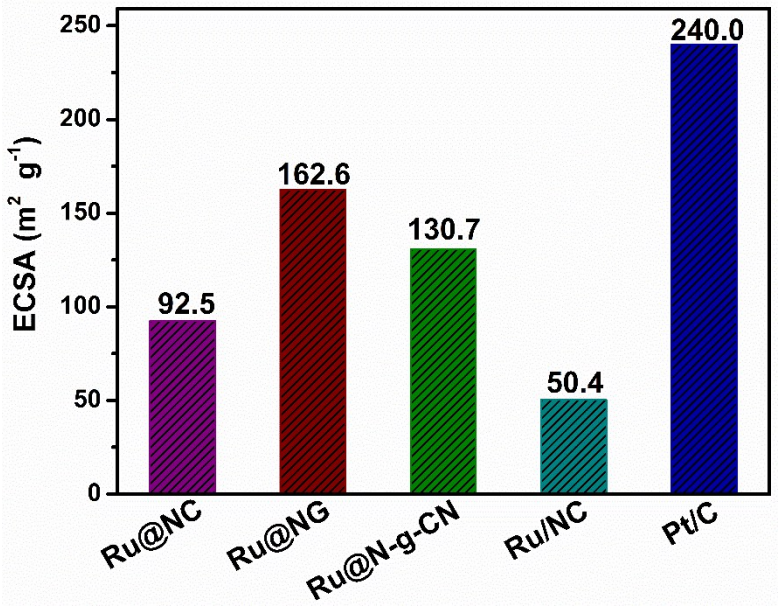

Figure. S23. The ECSA of Ru-based catalysts and Pt/C.

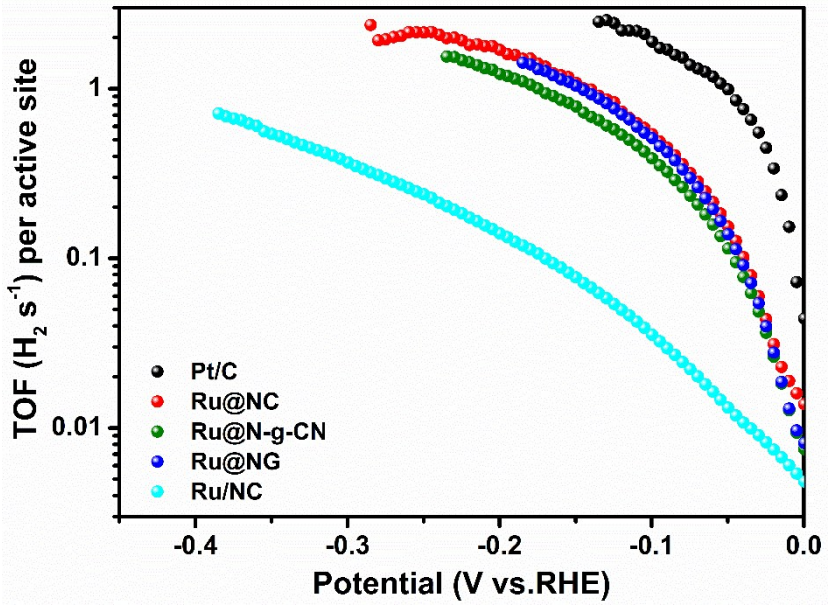

Figure. S24. TOF values of Ru-based catalysts and Pt/C in 0.5 M H_2SO_4 solution.

The electrochemical double layer capacitances (C_{dl}) of catalysts were measured by using a simple CV method. The C_{dl} value is expected to be linearly proportional to the electrochemically active surface area of the electrode.[4-5] A potential range of 0.15-0.25 V vs. RHE is selected for the capacitance measurements because no obvious electrochemical features corresponding to the Faradic current were observed in this region for all catalysts. Then, the capacitive currents of $\Delta J_{|Ja-Jc|}$@0.2V/2 were plotted as a function of the CV scan rate of 10, 20, 40, 60, 80, and 100 mV s^{-1}. These data are fit in a line, and the slope of which is the geometric C_{dl}.

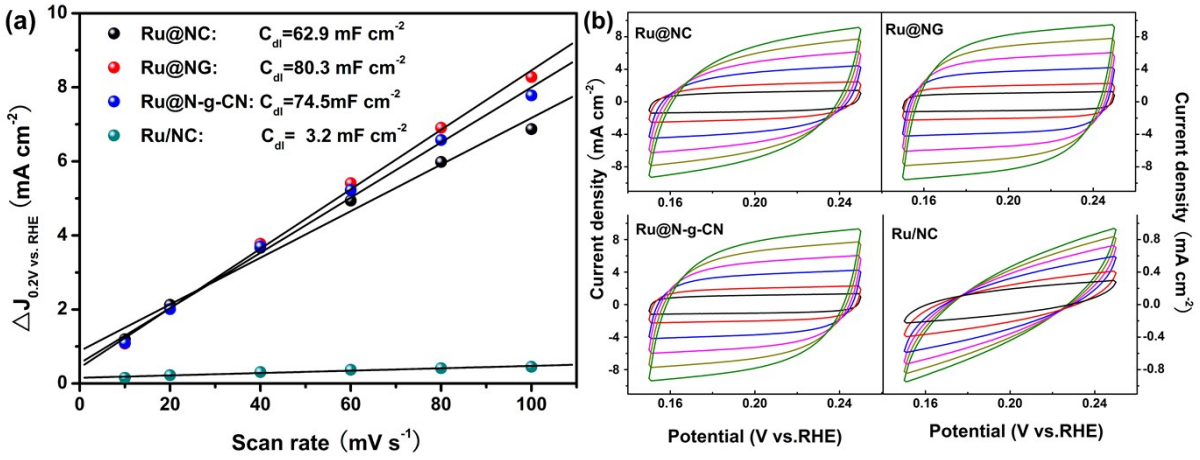

Figure. S25. (**a**) The calculated C_{dl} for Ru-based catalysts in 0.5 M H_2SO_4; (**b**) the corresponding CV curves in the range of 0.15-0.25 V vs. RHE where no faradaic reactions occurred.

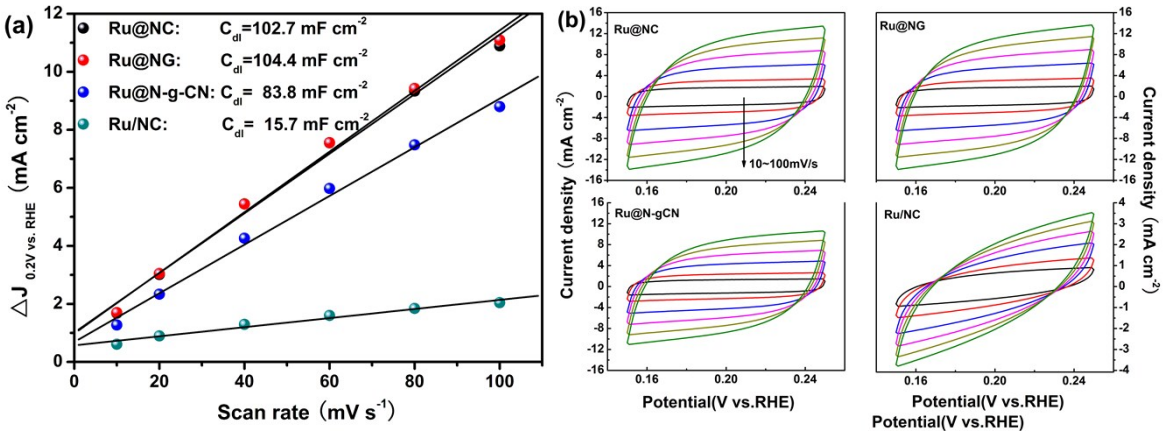

Figure. S26. (**a**) The calculated C_{dl} for Ru-based catalysts in 1.0 M KOH; (**b**) the corresponding CV curves in the range of 0.15-0.25 V vs. RHE where no faradaic reactions occurred.

The calibration of Ag/AgCl (saturated KCl) reference electrode was performed in corresponding electrolyte with a Pt plate as the working electrode, a Pt wire as counter electrode. The electrolyte maintains saturated condition with high purity hydrogen (99.999%). In 0.5M H_2SO_4, the potential was scanned from -0.30 to -0.2 V *vs.* Ag/AgCl at a scan rate of 5 mV s^{-1} and the corresponding cyclic voltammogram (CV) was recorded as below. The average of the two potentials at zero current was taken as the thermodynamic potential for the hydrogen electrode reactions.[6-7]

The RHE potentials were calculated:

E(RHE) = E(vs. Ag/AgCl)+0.212 V in 0.5 M H_2SO_4 (PH=0.30, measured by PHS-3C pH meter, Shanghai INESA Scientific Instrument Co., Ltd),

E(RHE) = E(vs. Ag/AgCl)+1.024 V in 1.0 M KOH (PH=13.89),

E(RHE) = E(vs. Ag/AgCl)+0.616 V in 1.0 M PB (PH=7.05).

If the RHE potentials were calculated by Nernst equation, then:

In acidic, E(RHE)= E(vs. Ag/AgCl)+0.215V (~ 3mV error Versus above-mentioned value);

In alkaline, E(RHE)= E(vs. Ag/AgCl)+ 1.019V (~ 5mV error);

In neutral, E(RHE)= E(vs. Ag/AgCl)+ 0.614 V (~ 2mV error).

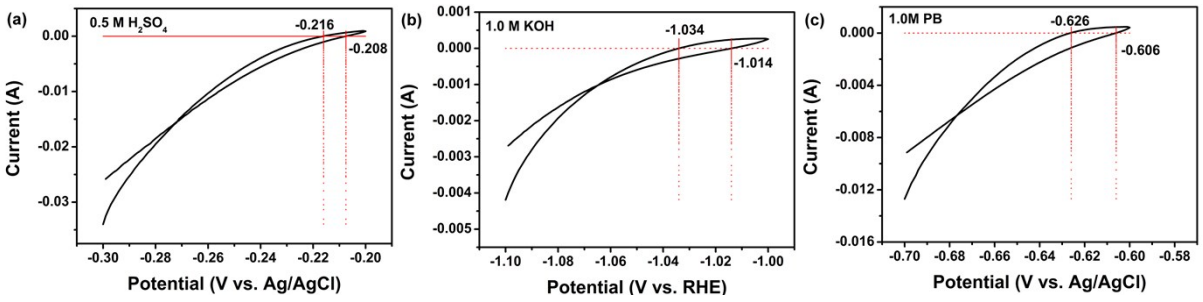

Figure. S27. The CV curves were recorded under acidic(**a**), alkaline (**b**) and neutral (**c**) conditions.

Table S**1. HER parameters of the reported comparable catalysts.**

Catalyst	Electrolyte	Current density (mA cm^{-2})	Overpotential at corresponding (mV)	Tafel slope (mA dec^{-1})	References
Ru@NC	0.5 M H_2SO_4	10	55.7	56	This work
		25	93.7		
		50	138.7		
	1.0 M KOH	10	25.3	29	
		25	55.3		
		50	102.3		
	1.0 M PB	10	165	171	
Ru@NG	0.5 M H_2SO_4	10	42.7	55	
		25	69.7		
		50	101.7		
	1.0 M KOH	10	20.3	26	
		25	41.3		
		50	72.3		
	1.0 M PB	10	128	120	
Ru@N-g-CN	0.5 M H_2SO_4	10	43.7	55	
		25	73.7		
		50	108.7		
	1.0 M KOH	10	19.3	29	
		25	39.3		
		50	70.3		
	1.0M PB	10	144	133	
Ru@C_2N	0.5 M H_2SO_4	10	22	30	8
	1.0 M KOH	10	17	38	
RuP_2@NPC	0.5 M H_2SO_4	10	38	38	9
	1.0 M KOH	10	52	87	
	1.0 M PBS	10	57	69	
S-4 (Ru-Co)	1.0 M KOH	10	52	69	10
Ru/C_3N_4/C	0.1 M KOH	10	79	/	3
Ru/NG-850	0.5 M H_2SO_4	10	22	30	11
Ru/GLC	0.5 M H_2SO_4	10	35	46	12
5.2wt% Rh-MoS_2	0.5 M H_2SO_4	10	47	24	13
Pt_3Ni_2-NWs-S/C	1.0 M KOH	10	42	/	14
		37.2	70		
Pt_2Pd/NPG700	0.5 M H_2SO_4	10	58	31	15

Table S2. **TOF parameters of the Ru-based catalysts in acidic and alkaline electrolyte.**

electrolyte	Overpotential (mV)	**TOF (H_2 s^{-1})**				
		Pt/C	Ru@NC	Ru@N-g-CN	Ru@NG	Ru/NC
0.5 M H_2SO_4	25	0.448	0.0447	0.039	0.042	0.008
	50	1.007	0.160	0.118	0.144	0.013
	100	1.954	0.544	0.399	0.519	0.036
1.0 M KOH	25	0.177	0.177	0.128	0.141	0.021
	50	0.437	0.437	0.306	0.338	0.029
	100	0.947	0.947	0.667	0.776	0.058

Reference

1. K. S. Lokesh and A. Adriaens, *Dyes and Pigments*, 2013, **96**, 269-277.
2. C. L. Green and A. Kucernak, *J. Phys. Chem. B*, 2002, **106**, 1036-1047.
3. Y. Zheng, Y. Jiao, Y. Zhu, L. H. Li, Y. Han, Y. Chen, M. Jaroniec and S. Z. Qiao, *J. Am. Chem. Soc.*, 2016, **138**, 16174-16181.
4. J. Yang, C. Cai, Y. Li, L. Gao, H. Guo, B. Wang, B. Pu and X. Niu, *Electrochimica Acta*, 2018.
5. Q. Han, Z. H. Cheng, J. Gao, Y. Zhao, Z. P. Zhang, L. M. Dai and L. T. Qu, *Adv. Funct. Mater.*, 2017, **27**, 1606352.
6. H. Lv, Z. Xi, Z. Chen, S. Guo, Y. Yu, W. Zhu, Q. Li, X. Zhang, M. Pan, G. Lu, S. Mu and S. Sun, *J. Am. Chem. Soc.*, 2015, **137**, 5859-5862.
7. Y. Liang, Y. Li, H. Wang, J. Zhou, J. Wang, T. Regier and H. Dai, *Nat. Mater.*, 2011, **10**, 780-786.
8. J. Mahmood, F. Li, S. M. Jung, M. S. Okyay, I. Ahmad, S. J. Kim, N. Park, H. Y. Jeong and J. B. Baek, *Nat. Nanotechnol.*, 2017, **12**, 441-446.
9. Z. Pu, I. S. Amiinu, Z. Kou, W. Li and S. Mu, *Angew. Chem. Int. Ed.*, 2017, **56**, 11559-11564.
10. J. Su, Y. Yang, G. Xia, J. Chen, P. Jiang and Q. Chen, *Nat. Commun.*, 2017, **8**, 14969.
11. R. Ye, Y. Liu, Z. Peng, T. Wang, A. S. Jalilov, B. I. Yakobson, S. H. Wei and J. M. Tour, *ACS Appl. Mater. Interfaces*, 2017, **9**, 3785-3791.
12. Z. Chen, J. Lu, Y. Ai, Y. Ji, T. Adschiri and L. Wan, *ACS Appl. Mater. Interfaces*, 2016, **8**, 35132-35137.
13. Y. F. Cheng, S. K. Lu, F. Liao, L. B. Liu, Y. Q. Li and M. W. Shao, *Adv. Funct. Mater.*, 2017, **27**, 1700359.
14. P. Wang, X. Zhang, J. Zhang, S. Wan, S. Guo, G. Lu, J. Yao and X. Huang, *Nat. Commun.*, 2017, **8**, 14580.
15. X. Zhong, Y. Qin, X. Chen, W. Xu, G. Zhuang, X. Li and J. Wang, *Carbon*, 2017, **114**, 740-748.